the Alq layers. These data indicate that holes can penetrate to some extent when the thickness of the *p*-EtTAZ layer is 30 Å, and the recombination zone locates both in the TPD and Alq layers. Thus, the recombination zone can be spatially controlled by adjusting the thickness of the *p*-EtTAZ layer, and emission from both the hole-transport layer (purplish blue) and the electron-transport layer (green) can be obtained with this device structure. These results are similar to the results obtained with another kind of a triazole derivative (*16*).

Because the device with a *p*-EtTAZ layer 30 Å thick provides bluish green light, the addition of red light should make the output white. To do so, we used the modulation doping technique developed by Tang *et al.* (*12*), in which the Alq layer is doped with Nile Red. Because the emissions from both Alq and Nile Red are necessary, a doped zone 50 Å thick is formed 50 Å away from the interface between the TPD and Alq layers. Thus, the excitons generated in the Alq layer near the interface between TPD and Alq diffuse to the doped layer, exciting the dopants. A TPD/Alq device designed in this manner displays emission from both Alq at 520 nm (green) and Nile Red at 600 nm (red), providing yellow light (Fig. 2, spectrum E). In this case, the dopant molecules are excited by the energy transfer from the host Alq or by direct excitation by carrier recombination at the dopant sites, or both.

Combining the spatial control of the recombination zone and the modulation doping technique, we attempted the generation of white light. The device structure is ITO/TPD (400 Å)/*p*-EtTAZ (30 Å)/Alq (50 Å)/Nile Red–doped (1 mol %) Alq (50 Å)/Alq (400 Å)/Mg:Ag (Fig. 1). Upon the application of dc voltage at ITO positive, white light is observed from the device through the glass substrate (Fig. 3). The EL spectrum (Fig. 2, spectrum F) covers a wide range of the visible region, and three peaks at 410, 520, and 600 nm are seen, corresponding to emission from TPD, Alq, and Nile Red, respectively. In Fig. 4, luminance-voltage and current-voltage characteristics are given. Luminescence starts at a low voltage, such as 6 V, and a maximum luminance of 2200 cd/m$^2$ is achieved at 16 V. In comparison, the luminance of a cathode ray tube monitor is about 100 cd/m$^2$. A reasonably high luminous efficiency of 0.5 lm/W is obtained at 12 V. At this drive voltage, the luminance is about 300 cd/m$^2$. Optimization of the device structure and the use of more suitable materials should provide higher efficiencies, as well as luminance that may exceed 8000 cd/m$^2$, the luminance of common fluorescent lamps.

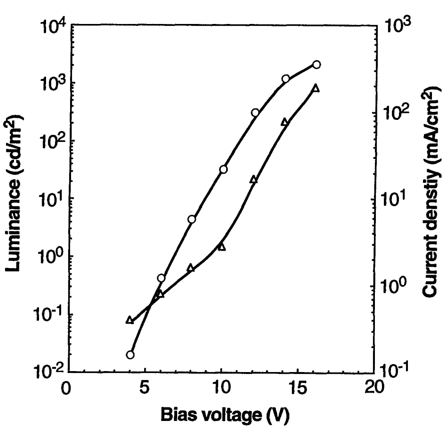

**Fig. 4.** Luminance-voltage (circles) and current-voltage (triangles) characteristics of a white light–emitting EL device. Luminance was measured at room temperature with a Minolta LS-100 luminance meter.

We have not measured the lifetime of the device yet; but in general, the stability of organic EL devices have been improving these days. Ten thousand hours of continuous operation has been reported (*22*). Because organic materials have flexibility in material design, an unlimited number of organic materials can be synthesized for the EL application, which is one of their major advantages over inorganic materials. Thus, the possibility of developing organic EL devices having practical durability is quite high.

## REFERENCES AND NOTES

1. C. W. Tang and S. A. VanSlyke, *Appl. Phys. Lett.* **51**, 913 (1987).
2. C. Adachi, T. Tsutsui, S. Saito, *ibid.* **56**, 799 (1990).
3. J. H. Burroughes *et al.*, *Nature* **347**, 539 (1990).
4. J. Kido, K. Nagai, Y. Okamoto, T. Skotheim, *Chem. Lett.* **1991**, 1267 (1991).
5. ______, *Appl. Phys. Lett.* **59**, 2760 (1991).
6. Y. Hamada, C. Adachi, T. Tsutsui, S. Saito, *Jpn. J. Appl. Phys.* **31**, 1812 (1992).
7. N. C. Greenham *et al.*, *Nature* **365**, 628 (1993).
8. E. Aminaka, T. Tsutsui, S. Saito, *Jpn. J. Appl. Phys.* **33**, 1061 (1994).
9. J. Kido, K. Hongawa, K. Okuyama, K. Nagai, *Appl. Phys. Lett.* **63**, 2627 (1993).
10. C. Adachi, S. Tokito, T. Tsutsui, S. Saito, *Jpn. J. Appl. Phys.* **27**, L268 (1988).
11. ______, *ibid.*, p. L713.
12. C. W. Tang, S. A. VanSlyke, C. H. Chen, *J. Appl. Phys.* **65**, 3610 (1989).
13. C. Adachi, T. Tsutsui, S. Saito, *Appl. Phys. Lett.* **55**, 1489 (1989).
14. J. Kido, M. Kohda, K. Okuyama, K. Nagai, *ibid.* **61**, 761 (1992).
15. J. Kido, M. Kohda, K. Hongawa, K. Okuyama, K. Nagai, *Mol. Cryst. Liq. Cryst.* **227**, 277 (1993).
16. J. Kido, C. Ohtaki, K. Hongawa, K. Okuyama, K. Nagai, *Jpn. J. Appl. Phys.* **32**, L917 (1993).
17. J. Kido, K. Hongawa, K. Okuyama, K. Nagai, *Appl. Phys. Lett.* **64**, 815 (1994).
18. M. Era, S. Morimoto, T. Tsutsui, S. Saito, *ibid.* **65**, 676 (1994).
19. V. L. Colvin, M. C. Schlamp, A. P. Alivisatos, *Nature* **370**, 354 (1994).
20. C. Morishima, M. Yoshida, A. Fujii, Y. Ohmori, K. Yoshino, *Jpn. J. Appl. Phys.* **33**, L1228 (1994).
21. J. Kido, H. Hayase, K. Hongawa, K. Nagai, K. Okuyama, *Appl. Phys. Lett.* **65**, 2124 (1994).
22. Y. Shirota *et al.*, *ibid.*, p. 807.

21 October 1994; accepted 23 December 1994

---

# A Structure Model and Growth Mechanism for Multishell Carbon Nanotubes

S. Amelinckx,* D. Bernaerts, X. B. Zhang, G. Van Tendeloo, J. Van Landuyt

A model that postulates a mixture of scroll-shaped and concentric, cylindrical graphene sheets is proposed to explain the microstructure of graphite multishell nanotubes grown by arc discharge. The model is consistent with the observed occurrence of a relatively small number of different chiral angles within the same tubule. The model explains clustering in a natural way and is consistent with the observation of asymmetric (0002) lattice fringe patterns and with the occurrence of singular fringe spacings larger than *c*/2 (*c* is the *c* parameter of graphite) in such patterns. Anisotropic thermal contraction accounts for the 2 to 3 percent increase in the *c* parameter of nanotubes, compared with bulk graphite, but is too small to explain the singular fringe spacings. The model also explains the formation of multishell closure domes. Nucleation is attributed to the initial formation of a fullerene "dome."

Iijima (*1*) found that nanometer-thin, micrometer-long tubes consisting of concentric, cylindrical graphene sheets are formed as a by-product of the arc-discharge synthesis of fullerenes (*2*). These tubes have a chiral character (*1*) that can determine their electronic properties (*3*). Electron diffraction studies showed that many multisheet tubules contain achiral as well as chiral tubes (*4*, *5*). A multilayer tubule may exhibit several chiral angles, their number being very often 1/2 to 1/5 the number of sheets, suggesting that the sheets occur in clusters with the same chirality. It was proposed (*4*, *5*) that the chirality is a means of accommodating

---

Electron Microscopy for Materials Research, University of Antwerp (RUCA), Groenenborgerlaan 171, B-2020 Antwerp, Belgium.

*To whom correspondence should be addressed.

the stepwise increase in circumference of successive tubes without disrupting the continuity of successive graphene sheets, while maintaining the graphite spacing between cylinders.

Certain tubules can exhibit an asymmetric fringe pattern; the average fringe spacing is larger in one wall section than in the other so that one wall appears thicker than the other. Moreover, the fringe patterns often show a mixture of two different spacings in one of the walls; the larger spacing is usually an isolated occurrence (*6*, *7*). These observations were attributed to the presence of a polygonal (pentagonal) cross section in the tubules (*7*, *8*). Polygonization had been postulated earlier as a second means of accommodating the stepwise increase in circumference, that is, "tilt" boundaries separating regions of more or less perfect graphitic stacking (*4*).

We propose an improved model for the multisheet tubules that accounts for the various observations made so far, in particular, the asymmetric fringe patterns. Zhang *et al.* have pointed out (*4*) that there is no compelling evidence for the concentric cylinder model, and they left open the possibility that the tubules might consist of scrolls rather than concentric cylinders. A scroll model was proposed for carbon fibers of more macroscopic dimensions (*9*). Simulations have shown that the scroll and cylinder images would be almost indistinguishable when viewed along a normal to the tubule axis (*10*). We propose a model incorporating elements of both types, and we suggest a growth mechanism that includes the nucleation stage. We discuss images that clearly support the scroll model. Growth models were reviewed in (*11*).

The growth scenario of a tubule can be formulated as follows. As already proposed (*4*), the nucleus can be a dome of the type occurring in the larger fullerene cages. A particular dome model giving rise to an achiral tube is shown in Fig. 1A, whereas Fig. 1B shows a chiral dome. Lateral extension by preferential growth along the rim of this dome would then give rise to a cylindrical tube in which the needle axis is parallel to, or encloses a small angle with, the direction of the C–C bonds of the curved graphene sheet (Fig. 2A), which agrees with the experimentally found geometry (the needle axis must be nearly parallel to [10$\bar{1}$0]*). A subsequent sheet, nucleated at the contact between substrate and initial dome (2 in Fig. 2B), will in general have to become chiral, even if the first tube is achiral, to form a cylinder. The helix angle depends to some extent on the requirement that a low-energy coincidence site interface is formed between successive graphite sheets. On growing laterally, sheet 3, which forms on top of this second chiral sheet as a template, will presumably tend toward a graphitic stacking with sheet 2, but it may not be able to do so because of the circumference increase, and as a result, a different chirality (larger or smaller) may have to be introduced to realize fit when completing the cylinder (Fig. 2, C and D).

At the prevailing growth temperatures, the graphene sheets can easily rearrange by sliding over one another (*12*), especially because "partial dislocations" are necessarily present between sheets (*4*). However,

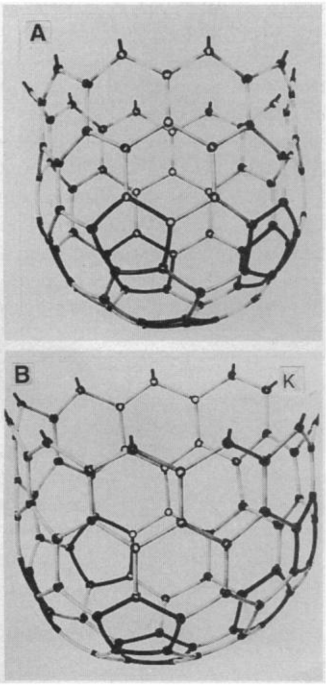

**Fig. 1.** Models of fullerene domes that can act as 3D nuclei for nanotubules. (**A**) Achiral half of a $C_{80}$ cage. (**B**) Chiral version of (A). Note the presence of a kink at K.

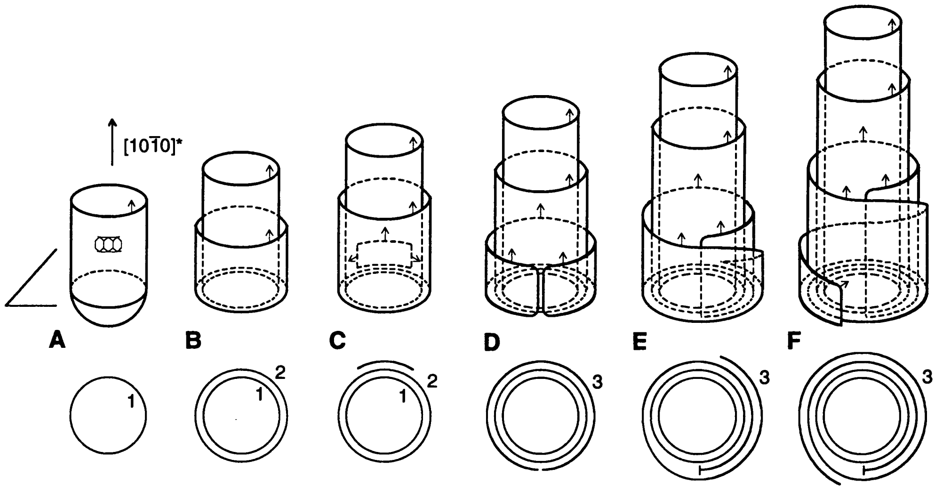

**Fig. 2.** Successive stages in the formation of a multishell graphite tube: spatial views and corresponding cross sections. (**A**) A fullerene dome is formed from a pentagonal cluster. If the dome is symmetrical, the initial tube (tube 1) is nonhelical; if the dome is chiral, then the initial tube will be chiral. (**B**) Sheet 2 is deposited on sheet 1 as a template; sheet 2 will in general be chiral even if sheet 1 is nonchiral. For clarity, the dome is omitted in this and subsequent drawings. (**C** and **D**) A 2D nucleus is formed and grows into a concentric cylinder. (**E**) Two edges of the 2D nucleus miss each other, and an edge dislocation is formed, giving rise to a scroll. (**F**) On further growth, the edge dislocation lengthens along the needle axis.

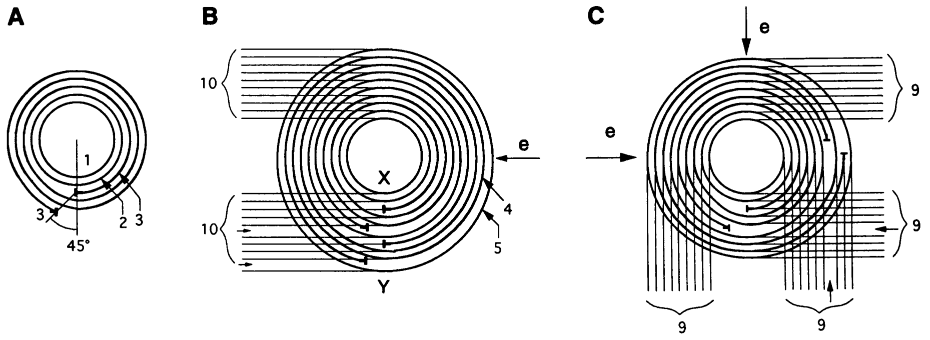

**Fig. 3.** Cross-sectional views. (**A** and **B**) The scroll generates several sheets with the same chiral angle, and a second scroll is formed. The image will exhibit 10 fringes in both walls. (**C**) Cross-sectional view of a nine-shell tubule containing two scroll-type defects. The lattice fringe patterns as viewed along two different incident electron beam directions are shown schematically. In both views a singular fringe spacing indicated by an arrow occurs in the image. The tubule will exhibit in general six different chiral angles.

the junction might fail to take place because of the large misfit along the meeting ledges that is due to the chirality induced by the underlying template. The two ledges might miss each other, and an edge-type Frank dislocation, roughly along the needle axis and with a Burger vector component normal to the sheets of *c*/2 (*c* is the *c* parameter of graphite), might form instead (Fig. 2E). This sheet (sheet 3) now becomes a chiral scroll, and its lateral growth may give rise to a number of sheets with the same chiral angle. The observed average number of layers in a cluster with the same chirality suggests that, after the formation of three to four spires, the probability for the two-dimensional (2D) nucleation of a new sheet becomes appreciable and competes with the lateral extension of the existing scroll sheet (Fig. 2F). This new sheet will again tend to form a graphitic stacking with respect to the underlying scroll-type sheet, which now functions as the new template. As it extends laterally, it may either form a cylinder or the same scenario may repeat, and after having formed a few turns of a scroll, a new sheet with a new chirality or without chirality may form.

This mechanism would generate a tubule containing pairs of edge dislocations of opposite signs, roughly parallel to the tube axis, that terminate successive scrolls. The configuration of least elastic interaction energy of such dislocation pairs is such that their connecting line forms an angle of 45° with the "glide" plane of the edge dislocations and such that the supplementary half-planes do not overlap (Fig. 3A) (*13*). These Frank dislocations are sessile, and they can rearrange either by climbing or by the cooperative glide of the whole sheet along the cylindrical surfaces, mediated by the glissile partial dislocations that must necessarily be present between successive sheets because of the circumference increase, as described in (*4*). The occurrence of a similar type of defect has already been postulated as a result of deintercalation experiments (*10*).

At high temperature, where the tubules are formed, the equilibrium configuration will likely be realized. In the band XY where the dislocations are present (Fig. 3B), the average *c* spacing will be increased because the repulsion between layers, as a response to a decrease in their separation, is larger than the attraction, opposing an increase in spacing resulting from the insertion of a supplementary half-plane. The attraction is due to weak van der Waals forces only. The same number of layers will still be observed in both parts, but one wall will be thicker than the other (Fig. 3B). Our model thus also provides a natural explanation for the sequence of different spacings, as observed, for instance, in (*6, 7*). More than one such dislocated zone, such as XY, may be present (Fig. 3C). Terminating 0002 fringes were occasionally observed in high-resolution images of onion-like particles (*7, 14, 15*). The difficulty of observing the cross section of straight tubules has hitherto prevented the observation of images revealing the structure presented in Fig. 3.

Somewhat less direct but nonetheless clear evidence can be obtained from images made normal to the tube axis. If the edge dislocation is not parallel to the tube axis, the singular fringe width will obtain its normal value at the point where the supplementary half-plane turns away from the edge-on orientation, which is required for imaging; simultaneously, the total width of the wall image decreases. This effect is shown in Fig. 4A. Figures 4B and 4C represent two cross sections at different levels of the tubule, illustrating the change in fringe spacing and wall thickness. An example is shown in Fig. 5, where in part X two singular fringe spacings acquire the normal width at two slightly different levels. There is also a corresponding change in the total width of the upper-wall image, which in certain parts is somewhat wider than the lower-wall image. In a quite different part of the same tubule (part Y), two singular fringe widths (arrows) appear again at precisely the same positions with respect to the wall surface shown in Fig. 5, part X, that is, between the same graphene sheets. The probability that this would happen by chance is negligible.

According to the concentric cylinder model, the "closure" of tubes can to some extent be considered as the inverse of the nucleation process: a dome or a set of concentric domes is generated by the formation of pentagons (*16*). The tubules containing a scroll can close as well, although the geometry is more difficult to visualize. The simplest case to represent is a conical termination, as shown in Fig. 6. The termination cone consists of a single sheet wound onto a conical helical surface. Its geometry is similar to that of conically wound graphite needles (*17*). The number of sheets in the termination will be equal to the number of spires in the scroll. The model implies that sheets belonging to the same scroll, that is, having the same chirality, will become closed simultaneously in a multishell cap. However, the reverse need not be true; sheets that become closed simultaneously do not necessarily belong to a scroll. Actual terminations of scrolls will obviously have shapes derived from a fullerene dome rather than from a simple cone as represented here for reasons of clarity only. Their topological features will be the same, however.

In his discussion of the growth mechanism, Iijima (*1, 18*) did not address explicitly the crucial problem of nucleation. He assumed [figure 10 in (*18*)] that a short cylindrical tube segment was already present but did not specify how it was generated.

Kinks in growth steps in general and kinks in the edges of graphene sheets in particular are preferred sites for the addition of carbon atoms on further growth (*18*). According to Iijima (*1, 18*), the "geometri-

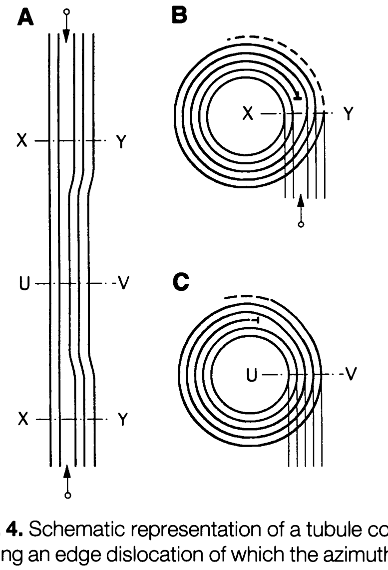

**Fig. 4.** Schematic representation of a tubule containing an edge dislocation of which the azimuthal position changes (**A**). Note the singular fringe separation in parts of one of the walls (arrows). Cross-sectional views XY and UV are represented at three different levels (**B** and **C**).

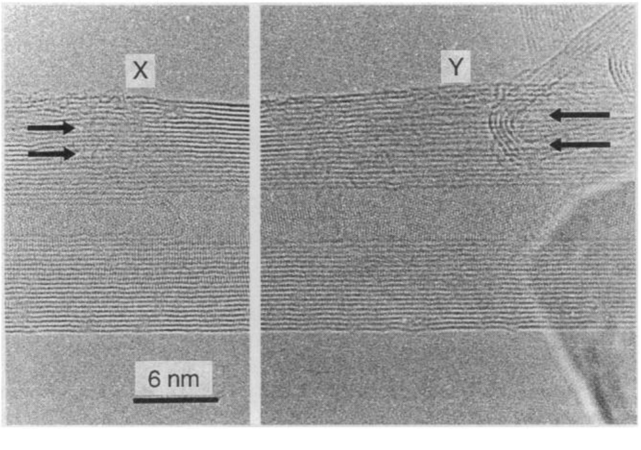

**Fig. 5.** Two parts of the same tubule (X and Y) containing two singular fringe separations indicated by arrows. The two singular fringes occur between the same graphene sheets in both places.

cal" kinks due to the chiral character of the graphene sheets are the only active growth sites. However, at the growth temperature the equilibrium concentration of thermal kinks should be large enough to ensure lateral growth of the sheets even in the absence of "geometrical" kinks. Nucleation of 2D islands followed by lateral growth should also be possible once the initial tube is formed, and the resulting tube can serve as a substrate; 2D nucleation is also required for the helical growth mechanism in the case of multilayer tubules. Such 2D nucleation can be heterogeneous and could take place at the contact between the substrate and the already existing tube, as was explicitly assumed in (*4*) and implicitly also in (*18*). Where the edges of an island meet in the process of forming a cylinder (Fig. 2D), this can lead to a misfit of the type represented in Fig. 7A. A relative shear, as indicated by arrows S, can eliminate this misfit, changing the chirality.

Alternatively, the misfit can be eliminated by the stacking of the right part on top of the left part so as to achieve the graphite stacking mode to create an edge dislocation (Fig. 7B). The latter process may be favored if geometrical constraints in the 2D nucleus impede the relative shear, for instance, due to the reentrant part of the tubule at the contact between dome and substrate (Fig. 7C). The step that was buried (Fig. 2E) on forming the dislocation is no longer supplied with carbon atoms and will no longer change its azimuth; on further growth it can only lengthen in the direction of the needle axis (Fig. 2, E and F). The dislocation line will thus become preferentially parallel to the tubule axis.

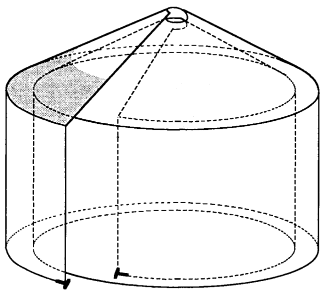

**Fig. 6.** Closure of a scroll-type part of a tubule. For clarity, the closing dome is represented as a simple cone; it consists of a single, conically wound graphene sheet.

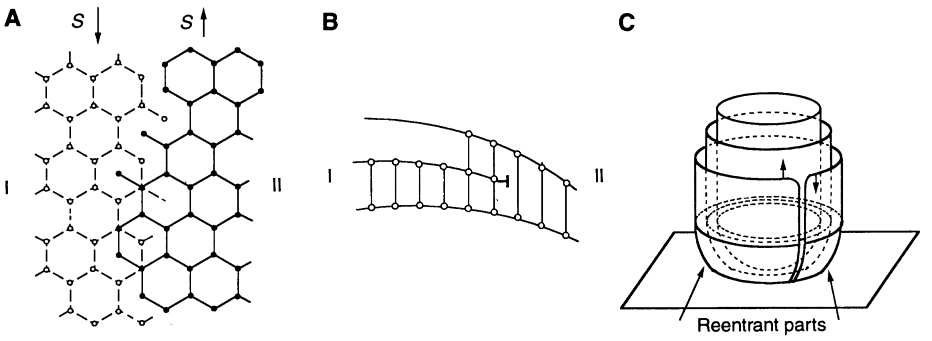

**Fig. 7.** Formation of a Frank-type edge dislocation where the two ledges of graphene sheets I and II meet. The misfit could be eliminated by a shear *S* along the common lattice plane of the two parts I and II (**A**) or by realizing a graphite stacking with formation of an "edge" dislocation (**B**). Shearing is impeded by reentrant parts at the contact between the substrate and the graphene sheet (**C**).

We now discuss in more detail possible 3D nuclei. It seems difficult to imagine conditions under which a graphene sheet would spontaneously roll up into a cylinder. Tubes form under the same physicochemical conditions under which closed carbon cages such as $C_{60}$, $C_{70}$, and the like form. It therefore seems reasonable to assume that the nucleus for the initial tube is a "dome," that is, a fullerene-type cage cut in half, limited by a circular or polygonal edge (Fig. 1). The dome in Fig. 1A has fivefold symmetry and is achiral. The dome in Fig. 1B has chiral character. Both domes are derived from a $C_{80}$ cage. According to our model, the size of the innermost tube is determined by the equator of the dome. To generate a tubular surface, the dome must contain six pentagonal meshes, which is half the number required for a closed convex fullerene cage. Also, the pentagon isolation rule must be satisfied. To be in agreement with the observed tubule texture, the equator must consist of a belt of hexagons having one set of C–C bonds either perpendicular to the rim or enclosing a small angle (the helix angle) with the normal to the rim. The smallest domes consistent with these requirements are derived from $C_{80}$ and would produce tubes with diameters of 7.85 or 8.2 Å, respectively, for achiral and chiral domes (Fig. 1, A and B). The smallest observed tubule diameter (~7 Å) (*19*) is in reasonable agreement with this prediction. Tubes with larger diameters would be based on domes derived from fullerene cages of the same symmetrical type as $C_{80}$, with numbers of carbon atoms given by $20k^2$ ($k$ is an integer), where $k - 1$ is the number of hexagons separating two adjacent pentagons. As a result, the diameters of tubules should be "quantized" in a specific manner. This would provide an indirect way of verifying the present nucleation model.

As an alternative explanation for the singular fringe widths, one might think of the large anisotropic thermal contraction of graphite and the geometrical constraints due to the cylindrical shape. At the formation temperature (~3000 to 4000 K), the difference in the length of the circumferences of two successive cylinders, $\pi c$, is compatible with their difference in radii, $1/2c$. However, this is no longer true at the observation temperature as a result of the anistropic thermal contraction on cooling. The length changes of the circumferences are determined by the relative contraction $\Delta \ell / \ell = -\alpha_{\parallel} \Delta T$, where $\alpha_{\parallel}$ is the thermal expansion coefficient parallel to the basal planes and $T$ is temperature. The length changes along the radial directions are governed by the relation $\Delta r / r = -\alpha_{\perp} \Delta T$, where $\alpha_{\perp}$ is the thermal expansion coefficient along the normal to the basal planes. In graphite we have $\alpha_{\parallel} \ll \alpha_{\perp}$, and the change in the radius difference is larger than required by the change in the length difference of the circumferences. As a result, a compressive thermal stress operates along a tangential direction and a tensile stress along the radial direction. The latter tends to increase the $c$ parameter, whereas the former tends to decrease the $a$ parameter. Because graphite is elastically much stiffer in a direction parallel to the graphene sheets (covalent bonding) than perpendicular to them (van der Waals bonding), the $c$ parameter would increase relative to its value in the bulk, at the same observation temperature, but the $a$ parameter would change little ($\Delta c/c \approx 0.03$ to $0.04$) (*20*). An increase in the $c$ parameter of this order of magnitude was found in nanotubes as compared with the $c$ parameter of bulk graphite (*6, 21*).

Although the effect was attributed to turbostratic disorder (*21*), it is more likely due to thermal stresses. For our purposes it is sufficient to note that the effect is too small to account for the observed density of singular fringe spacings. Moreover, one would expect the thermal effect to be spread uniformly over the entire tubule thickness, rather than being localized between certain sheets only. Furthermore, it should occur in all sufficiently thick tube walls, which is not the case for the singular fringe spacings. Image formation at an angular bend of a polygonal tube as proposed in (*7*) can account for a spacing increase for all fringes in one-half of the image, but not for the occurrence of a few singular fringe widths.

Evidence, such as a surface step along the edge of a sheet, could in principle be obtained by scanning tunneling or atomic force microscopy, but, to our knowledge, no such evidence has been published. Geometrical factors, as well as the absence of clean surfaces, seriously hamper such observations.

## REFERENCES AND NOTES

1. S. Iijima, *Nature* **354**, 56 (1991).
2. R. F. Curl and R. E. Smalley, *Sci. Am.* **265**, 32 (October 1991).
3. M. S. Dresselhaus, G. Dresselhaus, R. Saito, *Phys. Rev. B* **45**, 6234 (1992).
4. X. F. Zhang *et al.*, *J. Cryst. Growth* **130**, 368 (1993).
5. X. B. Zhang, X. F. Zhang, S. Amelinckx, G. Van Tendeloo, J. Van Landuyt, *Ultramicroscopy* **54**, 237 (1994).
6. Z. G. Li, P. J. Fagan, L. Liang, *Chem. Phys. Lett.* **207**, 148 (1993).
7. M. Liu and J. M. Cowley, *Ultramicroscopy* **53**, 333 (1994).
8. ______, *Carbon* **32**, 393 (1994).
9. R. Bacon, *J. Appl. Phys.* **31**, 283 (1960).
10. O. Zhou *et al.*, *Science* **263**, 1744 (1994).
11. T. W. Ebbesen, *Annu. Rev. Mater. Sci.* **24**, 235 (1994).
12. J. C. Charlier and J. P. Michenaud, *Phys. Rev. Lett.* **70**, 1858 (1993).
13. A. M. Kosevich, in *Dislocations in Solids*, F. R. N. Nabarro, Ed. (North-Holland, Amsterdam, 1979), vol. 1, pp. 66–67.
14. L. Margulis, J. L. Hutchison, R. Tenne, in *Electron Microscopy 1994*, proceedings of the *13th International Conference on Electron Microscopy*, Paris, 17 to 22 July 1994, B. Jouffrey and C. Colliex, Eds. (Les éditions de physique, Paris, 1994), vol. 2A, p. 317.
15. V. P. Dravid *et al.*, *Science* **259**, 1601 (1993).
16. P. M. Ajayan, T. Ichihashi, S. Iijima, *Chem. Phys. Lett.* **202**, 384 (1993).
17. S. Amelinckx, W. Luyten, T. Krekels, G. Van Tendeloo, J. Van Landuyt, *J. Cryst. Growth* **121**, 543 (1992).
18. S. Iijima, *Mater. Sci. Eng. B* **19**, 172 (1993).
19. ______ and T. Ichihashi, *Nature* **363**, 603 (1993).
20. The order of magnitude of the relative change in the *c* parameter due to stresses will be at most $(\alpha_\perp - \alpha_\parallel)\Delta T$. With $\alpha_\perp - \alpha_\parallel \approx 10^{-5}$/K [B. T. Kelly, in *Materials Science and Technology*, R. W. Cahn, P. Haasen, E. J. Kramer, Eds. (VCH, Weinheim, 1994), vol. 10A, part I, p. 383] and $\Delta T \approx 3 \times 10^3$ to $4 \times 10^3$ K, one finds $\Delta c/c \approx 0.03$ to 0.04.
21. Y. Saito, T. Yoshikawa, S. Bandow, M. Tomita, T. Hayashi, *Phys. Rev. B* **48**, 1907 (1993).

22. This work was funded in part by the Belgian National Program of Inter-University Research Projects initiated by the State Prime Minister Office (Science Policy Programming). We also acknowledge funding from the National Fund for Scientific Research.

2 September 1994; accepted 6 December 1994

---

# Synthesis and Characterization of Anisometric Cobalt Nanoclusters

Charles P. Gibson* and Kathy J. Putzer

Sonication of aqueous $Co^{2+}$ and hydrazine resulted in the formation of anisometric (disk-shaped) cobalt nanoclusters that averaged about 100 nanometers in width and 15 nanometers in thickness. Electron diffraction from single particles revealed that they were oriented (001) crystals that conformed to a trigonal or hexagonal unit cell four times the size of the cell adopted by bulk α-cobalt. Lorentz microscopy indicated that these were single–magnetic domain particles, with the axis of magnetization located in the (101) plane, offset at some appreciable angle from the ⟨001⟩ axis.

Small magnetic particles (magnetic nanoclusters) are of immense technological importance because of their use in magnetic recording media and in the construction of permanent magnets (*1*, *2*). Desirable characteristics for these materials include sufficient shape and magnetocrystalline anisotropy so that a preferred magnetic field orientation is adopted in the final product. Ideally, the nanoclusters would be monodisperse and magnetically hard, and each particle would contain a single magnetic domain.

Of the three transition metals that are normally ferromagnetic (Fe, Co, and Ni), oriented nanoclusters of cobalt probably have the greatest potential for use because α-cobalt (unlike iron and nickel) is uniaxial (*2*, *3*). Unfortunately, however, facile syntheses leading to anisometric cobalt nanoclusters have not yet been reported (*4*). Herein we describe such a synthesis: a facile and inexpensive procedure that leads to oriented, anisometric, single-domain ferromagnetic cobalt nanoclusters.

Initial attempts to synthesize colloidal cobalt at moderate temperature (≤100°C) by reduction of $Co^{2+}$(aq) with hydrazine were unsuccessful, presumably because of the kinetic stability of the system (*5–7*). Because the attempted reaction was, in theory, thermodynamically allowed and quite exothermic (*7*, *8*), we reasoned that a self-sustaining reaction might be initiated by the application of high-intensity ultrasound.

When basic solutions containing $Co^{2+}$ and hydrazine were sonicated, there was, following a short induction period, a sudden color change (blue-violet to silver-gray) as a result of the formation of colloidal cobalt. The colloidal cobalt nanoclusters were allowed to flocculate and, under the influence of gravity, fall to the bottom of the reactor. Most of the liquid in the reactor was removed by means of a cannula and was then replaced with water. The particles were resuspended and allowed to flocculate and settle once again, whereupon most of the liquid was removed. This washing process was repeated until the pH of the removed water was between 7 and 8. At this point, the hydrated floc was either stored for later use or the water was removed under a stream of dry nitrogen (or under vacuum) to give a free-flowing gray powder (*9*, *10*). Both the hydrated floc and the free-flowing gray powder were ferromagnetic. Assays of the gray powder by atomic absorption and energy dispersive x-ray spectroscopy (EDS) showed that it consisted primarily of cobalt (98.3%). A small amount of oxygen was also present, presumably in the form of a very thin oxide coating (*10*, *11*). No other impurities were present in quantities measurable by EDS. Samples that were to be characterized by transmission electron microscopy (TEM), Lorentz electron microscopy, and selected area electron diffraction (SAD) were prepared from the hydrated floc. The floc was dispersed by sonication and then deposited on a Formvar or collodion-coated TEM grid.

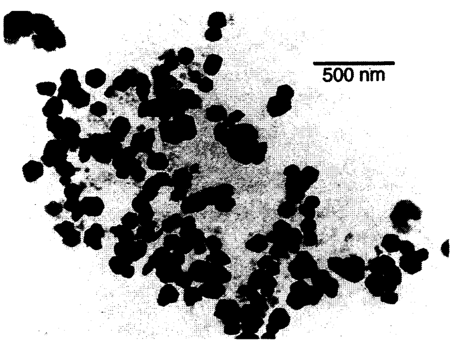

**Fig. 1.** A group of cobalt nanoclusters. The particles, which adopt a hexagonal or centered trigonal unit cell, are preferentially deposited as oriented (001) plates.

It is significant to note that, when handled properly, samples of the hydrated floc could be stored (under nitrogen) and effectively resuspended for at least several days after the initial synthesis. This property was a bit surprising because ferromagnetic particles tend to form tight aggregates as a result of magnetic attractions between the particles (*1*, *12*). However, the cobalt nanoclusters are small enough to be strongly influenced by Brownian forces. Because of the shape anisotropy of the particles, these forces result in the rotation of the particles (Brownian rotation). This effect probably inhibits the intimate contact between particles that is necessary for agglomeration (*13*, *14*).

Examination of the product by TEM revealed that it consisted of anisometric (disk-like) nanoclusters that were more or less hexagonal in shape. A photomicrograph of a typical product (Fig. 1) illustrates the morphology of the particles and shows their orientation with respect to the polymer-coated TEM grid. We see from this image that the

---

Department of Chemistry, University of Wisconsin, Oshkosh, WI 54901, USA.

*To whom correspondence should be addressed.